Version 17th July 2012

Atomic model of the human cardiac muscle myosin filament

by

Hind A. AL-Khayat[1]*, Robert W. Kensler[2], John M. Squire[3], Steve B. Marston[1]

and Edward P. Morris[4]

[1]National Heart and Lung Institute, Faculty of Medicine, Imperial College London, London W12 0NN, U.K.

[2]Department of Anatomy, University of Puerto Rico Medical School, San Juan, Puerto Rico 00936-5067, U.S.A.

[3]School of Physiology & Pharmacology, University of Bristol, Bristol BS8 1TD, U.K.

[4]The Institute of Cancer Research, 237 Fulham Road, Chester Beatty Laboratories, London SW3 6JB, U.K.

***Corresponding Author**

E:mail h.al-khayat@imperial.ac.uk

Running Title: Myosin filaments in human cardiac muscle

ABSTRACT

We have carried out the first 3D single particle analysis of electron micrograph (EM) images of negatively stained myosin filaments isolated from human cardiac muscle in the normal (undiseased) relaxed state. The resulting 28 Å resolution 3D reconstruction showed both axial and azimuthal (no radial) myosin head perturbations within the 429 Å repeat, with rotations between successive 140 to 150 Å-spaced crowns of approximately 60°, 35° and 25° compared to the values of 40˚, 40˚, 40˚ for a truly helical unperturbed 3-stranded structure. We have defined the myosin head atomic arrangements within the three different levels as well as modelling the organisation of myosin S2 and the 39 Å-spaced domains of titin and cMyBP-C on the surface of the myosin filament backbone. Best fits were obtained with head conformations on all three crowns which were similar to, but slightly modified from the structure of the two-headed myosin molecule of vertebrate chicken smooth muscle in the dephosphorylated relaxed state. Individual crowns show differences in the tilts of the head pairs and in the orientation of S2 relative to the heads which together with the azimuthal and axial perturbations result in systematic variations in the interactions between myosin heads. Detailed analysis of these interactions together with those with cMyBP-C and titin will lead to the understanding of the structural effects of mutations in myosin, cMyBP-C and titin, known to be associated with human cardiomyopathies.

INTRODUCTION

Muscle contraction involves the interaction between actin and myosin filaments that leads to force production mediated by the hydrolysis of ATP. Myosin filaments are assemblies of myosin molecules and accessory proteins. Myosin molecules comprise two heavy chains and four light chains. They contain two elongated globular head domains formed from the N-terminal domain of the heavy chains together with two light chains. The myosin heads are attached to a 1500 Å-long rod-shaped tail domain made up of an α-helical coiled-coil formed from the C-terminal regions of the heavy chains. Myosin heads are ATPases that interact with actin filaments to produce force and movement (1). The region of the rod corresponding to the first 400 Å immediately adjacent to the heads is known as myosin subfragment-2 (S2). Myosin filaments are generally bipolar with the myosin tails packing together in an almost cylindrical backbone and the heads projecting out laterally in a helical or quasi-helical fashion at intervals of ~143 Å. In the myosin filaments of vertebrate striated muscles, the myosin heads are arranged in a 3-stranded quasi-helical array on the filament surface (2) with the accessory proteins titin (3, 4), myosin binding protein (MyBP-C, (5)) and possibly the MyBP-C analogue, X-protein (6), located on the surface of the backbone. MyBP-C is located within the C-zones of the myosin filament which are regions ~3500 Å long centrally located the two halves of the bipolar filament. Titin is an unusually large elongated protein (3.8 MDa) which runs parallel to the actin and myosin filaments and spans half the length of a sarcomere. It is composed of a linear array of immunoglobulin (Ig) and fibronection (Fn3) domains connected by short linkers. Within the C-zone the titin domains are distributed in a pattern corresponding to an eleven domain super-repeat every 429 Å repeat. In comparison, the cardiac isoform of MyBP-C (cMyBP-C) has a mass of ~140 KDa and is made up of a linear array of eleven Ig and Fn3 domains.

Myosin filament structure has been investigated both by electron microscopy and by X-ray fibre diffraction to explore the different organisation and properties of myosin filaments from a variety of organisms and tissues (7, 8). The most detailed structural description of a myosin filament derives from helical three-dimensional (3D) reconstruction of cryo-electron microscope images of tarantula myosin filaments at a resolution of ~25 Å (9, 10). In the tarantula myosin filament, pairs of myosin heads were identified forming a similar interaction to that found in the off state of vertebrate smooth muscle myosin (11). Vertebrate skeletal and cardiac myosin filaments differ from those in invertebrates such as tarantula in that the myosin

heads depart from an exact helical arrangement. Hence, for vertebrate skeletal and cardiac myosin filaments, helical reconstruction is not a valid approach for the analysis of electron microscope data. Working on a variety of myosin filaments we have developed an alternative method to determine 3D structures of myosin filaments from electron microscope data based on single particle analysis (12) which is well suited to the analysis of quasi-helical myosin filaments. We have applied the approach to myosin filaments from a variety of muscle types including vertebrate skeletal and cardiac muscles (13, 14) and invertebrate striated muscle (15). A similar approach has been used in the analysis of mouse cardiac myosin filaments (16): in the resulting structure myosin heads were also found to adopt a paired conformation similar to that in tarantula myosin filaments.

Mutations in human cardiac muscle myosin and its associated proteins, cMyBP-C and titin, are known to cause a number of human cardiomyopathies, such as familial hypertrophic cardiomyopathy and dilated cardiomyopathy (17, 18). A detailed knowledge of the structure of human cardiac myosin filaments in the normal (un-diseased) relaxed state is likely to be important in understanding how the mutations give rise to the cardiomyopathies. To address this issue we have successfully developed a laboratory method to isolate myosin filaments from human cardiac muscle that preserves the highly ordered pseudo-helical structure of the relaxed filaments, thus making them amenable to analysis by electron microscopy and single particle image analysis. From such samples we have produced a 3D reconstruction of the C-zone of the myosin filament at ~28 Å resolution which allows the detailed docking of myosin heads and the modelling of the constituent domains of titin and cMyBP-C.

RESULTS

Three-dimensional structure of the human cardiac myosin filament. Electron microscope images were recorded from negatively stained preparations of myosin filaments isolated from human ventricular muscle. From these images well preserved examples of myosin filaments were selected in which the C-zone could be clearly identified (Fig. S1A,B). Fourier analysis of the C-zones of such filaments showed good recovery of detail with the characteristic layer-line pattern arising from the quasi-helical myosin head distribution together with meridional reflections extending to ~27 Å (the 16^{th} order of the 429 Å repeat, Fig. S1C,D). From 237 myosin filament C-zones a total 1559 segments were extracted, each segment corresponding to two 429 Å repeats. An initial reference 3D structure

was calculated using C3 symmetry (threefold rotational symmetry) from a single class average of the segments. Starting from this reference a refined 3D structure was calculated from the individual segments by successive rounds of forward projection, multireference alignment and 3D reconstruction. During the refinement the number of segments was reduced to 285 by selecting only those which agreed most strongly with forward projections of the structure. The selected segments provide an even distribution of projection angles (Fig. S2). The final 3D reconstruction (Fig. 1), which has an estimated resolution of 28 Å (Fig. S3), is characterised by a considerable level of detail. Within the repeating unit of 429 Å there are three distinct sets of densities on the outer surface of the filament (Fig. 1A,B) which correspond to three crowns of myosin heads. The location of the crowns within the C-zone matches that described in earlier studies of vertebrate skeletal and cardiac muscle (13, 14) and they are labelled 1, 2 & 3 following the same convention. Here crown 1 is the most massive with its extra mass arising from MyBP-C (NB this is a different numbering scheme from that used by Zoghbi *et al*. (16) in their analysis of the mouse cardiac myosin filament where the equivalent crowns are labelled 1, 3 and 2). Each crown is made up of 3 pairs of myosin heads. Direct inspection of the density associated with each crown allows the recognition of myosin head pairs which form triangular motifs (Fig. 1C,D) very similar in appearance to the conformation of myosin head pairs in the off state of vertebrate smooth muscle myosin (Fig. 1E, (11)). Similar shapes were seen in the tarantula myosin filament reconstruction (9) where the base of each triangle oriented towards the M-band corresponds to the two motor domains and the two sides correspond to the lever arms.

Fitting the crown densities with myosin molecular models. Since we identified motifs in each of crowns with close resemblance to the myosin head pairs in tarantula myosin filaments we proceeded to dock the corresponding atomic model into the crown densities using URO (19). For this purpose we used 3DTP.pdb (10) (a modified version of the off state of vertebrate smooth muscle myosin, (11), which also includes part of the coiled-coil S2 structure). We found that the best fit within the density map could be obtained by uncoupling and separately docking the two S1 domains resulting in minor changes in the mutual interaction of the motor domains and minor reorientations of the lever arms. Nevertheless, in each case the overall structure of the docked head pair is not very different from the original structure (11) and had similar intra-molecular interactions between the motor domains of the blocked and free heads as described previously (11). We also found it necessary to reorient the S2. Fig. 2(A,C) show two different views of our best fit structure within the map. Overall the fitted coordinates correspond closely to the density while revealing characteristic features of the individual crowns. In crown 3 there is little density unaccounted for within the head pair motif and almost all the

coordinates are contained within the density. However, in the case of crown 1 there are minor excursions associated with the regulatory light chain (RLC) of the blocked head and the essential light chain (ELC) of the free head, while for both crowns 1 and 3, the N-terminal SH3 domains (residues 33 to 78) of both the blocked and free heads extend outside the density. This latter effect may be associated with the conformational variability observed in this region of myosin (20). On the other hand, in the case of crown 2, while the overall shape of the head pair conforms quite well with the fitted coordinates, there are regions where the coordinates lie outside the density more substantially, particularly at the N-terminal SH3 domains of the two heads and in the regions of the lever arms. The least density is recovered for the head domains in crown 2. This may arise because the heads in crown 2 are less well ordered than in crowns 1 and 3.

Myosin head arrangement in crowns 1, 2 and 3. The fitted positions of the myosin heads within the cardiac myosin filament (Fig. 2.B,D) can be used to characterise the pseudo-helical head arrangement of the filament as summarised in Table I. This gives the axial and angular displacements between successive crowns measured both between the centres of each head pair and between the ends of the lever arm at the C-terminal position of the S1 domains where they connect to S2. The azimuthal displacement represents the rotation about the filament axis between head pairs on successive crowns. Comparison of these parameters with the corresponding values for a regular 3-start helix with a repeat of 429 Å allows the perturbations from an exact helical structure to be accurately defined. For the axial displacements the values are very similar whether measured between the centres of the head pairs or between the ends of the lever arms: and it is apparent that crowns 1 and 2 are closer together (axial displacement ~133 Å) than either crowns 2 and 3 or crowns 3 and 1 (axial displacement ~148 Å). In comparison, an unperturbed helix would have a uniform axial displacement of 143 Å. On the other hand, the angular displacement between crowns 1 and 2 (60˚ measured between the centres of the head pairs, and 58˚ between the ends of the lever arms) is very much greater than the equivalent measurements between crowns 2 and 3 (35˚ and 30˚, respectively) and between crowns 3 and 1 (25˚ and 32˚, respectively). These values can be compared to an unperturbed helix which would have a constant azimuthal displacement of 40˚. Hence the head arrangement in the cardiac myosin filament is characterised by a sequence of 3 crowns (2,3,1) with similar axial displacements (~148 Å) and approximately similar angular displacements (~30˚). This is followed by a discontinuity in which the transition to the next crown has a reduced axial displacement (~133 Å), but a substantially increased angular separation (~60˚). This gives rise to the phenomenon in which the head pairs in the 2,3,1 crown sequence are quite closely connected along a pseudo-helical track, but due to the angular

discontinuity the connection with the next 2,3,1 sequence is not maintained. In addition to the variations in axial and angular displacements between adjacent crowns, the head pairs also exhibit a variation in their tilt angle. This can be most readily appreciated by comparing the orientation (or tilt angle) of the extended density arising from the two motor domains of each head pair. Here it is apparent that the crowns 2 and 3 have very similar orientations while in comparison crown 1 is rotated by 19^{o} in a clockwise direction. Despite these perturbations in axial displacement, azimuthal displacement and tilt, the radial perturbation of myosin heads is minor in the human cardiac myosin filament in agreement with previous observations for both the fish and rabbit myosin filaments (13, 14).

Interactions between the myosin heads. Independent docking of the heads within the head pairs in each crown leads to a similar intramolecular arrangement for the head pairs in which the intramolecular interactions observed in previous studies of smooth muscle myosin (11) and tarantula muscle (9, 10) are substantially conserved. In contrast, intermolecular interactions between the head pairs on adjacent crowns vary much more substantially (Fig. 3A). As noted above, the head pairs in the 2,3,1 crown sequence are quite closely connected, while there is a distinct gap between crowns 1 and 2 and these two head pairs do not appear to be connected (Fig. 3B). In contrast, the head pairs in crowns 2 and 3 are connected through an interaction between the ELC of the blocked head on crown 2 and the motor domain of the free head on crown 3 (Fig. 3C). A similar interaction was observed between heads in successive crowns in the purely helical tarantula myosin filament (9, 10). This structural similarity can be understood since the head pairs on crowns 2 and 3 both have the same tilt angles (Table 1). Moreover the angular rise between crowns 2 and 3 (35˚) in the human cardiac myosin filament is quite similar to the angular separation of 30˚ in tarantula and the axial spacing of 148 Å is also similar to that in tarantula (145 Å). A notably different type of intermolecular connection is observed between crowns 3 and 1. This is mediated by the interaction between the RLC of the blocked head on crown 3 and the motor domain of the free head on crown 1 (Fig. 3(D)). The different mode of interaction compared with that between crowns 2 and 3 can be considered as the consequence of the clockwise 19^{o} rotation of the head pair on crown 1 and the reduced angular rise between crowns 3 and 1 (25^{o}) both of which serve to shift the motor domain of the free head on crown 1 from the ELC to the RLC of the blocked head on crown 3. To our knowledge this type of interaction between myosin head pairs in adjacent crowns has not previously been described. Although, in their studies of mouse cardiac myosin filament, Zoghbi *et al*. (16) present a docking of myosin head pairs on crowns 3 and 1 (they call them crowns 2 and 1) in which the motor domain of the free head on

crown 1 can be seen to make contact with the RLC of the blocked head on crown 3, this is was not mentioned by the authors.

Location of S2. S2 was docked into the reconstruction separately from the myosin head pairs starting from the configuration observed in tarantula myosin filaments (9, 10) (Fig. 2A,C). Furthermore, the variation in tilt angle of the head pairs on different crowns required S2 to be further subdivided into the segment running from the end of the lever arms to the blocked motor domain (residues 854 to 927 of S2) and the remaining C-terminal segment (residues 928 to 972 of S2). Although not fully resolved from the rest of the density of the head pair, the proximal region of S2 can be accommodated within crown 3 where it is integrated with the density of the lever arms of the blocked heads. A similar location with respect to the myosin heads for the proximal region of S2 was obtained in the case of crown 1, although in this case it is not fully accommodated in the density. These conformations are very similar to that observed in tarantula myosin filament (9, 10) suggesting that the intramolecular interaction between S2 and the actin binding domain of the blocked motor domain may be conserved between tarantula and human cardiac myosin filaments. The less complete recovery of myosin head pair density on crown 2, noted above, also applies to this segment of S2. For consistency, given the fact that the head pairs on level 2 have the same tilt angle as the head pair on level 3, the S2 is docked in a similar conformation to head 3, but not accommodated in the density. The distal regions of S2 in all the three crowns are accommodated in density and run close to the surface of the myosin filament backbone running approximately parallel to the filament axis.

Location of non-myosin protein densities: titin and cMyBP-C. Having identified the density in the structure of the human cardiac myosin filament which can be ascribed to the myosin heads and S2, we could now seek to identify the non-myosin components. Alongside the 2,3,1 crown sequence of myosin heads with strong intermolecular interactions, the myosin filament is characterised by regions with prominent and well defined surface features with a regular modulation every 40 Å consistent with the size of the Ig and Fn3 domains of titin and cMyBP-C (Fig. 4). Accordingly we sought to develop models of titin and cMyBP-C to fit these densities.

Titin is thought to extend from the Z-band (N-terminus) to the M-band (C-terminus), with six titin strands per half thick filament (21, 22) and it is likely that the six titins are grouped as three strands of titin pairs. Titin Ig and Fn3 domains are arranged in long-range patterns or super-repeats. Within the myosin filament bridge region, two types of titin super-repeats are found. There are 7

consecutive copies of the seven-domain 'small' super-repeat in the D-zone at the distal edge of the A-band. These are followed by 11 copies of the eleven-domain 'large' super-repeat. The eleven-domain repeats each follow the sequence -Ig-Fn3-Fn3-Ig-Fn3-Fn3-Fn3-Ig-Fn3-Fn3-Fn3-. The axial distance between each 'large' super-repeat copy is 429 Å and this series ends at the edge of the bare zone; (23-26). The 11 copies of the eleven-domain 'large' super-repeat of titin cover both the C-zone and the P-zone (Fig. S1B). cMyBP-C is a modular structure comprising eleven Fn3 and Ig domains (C0-C10) (27, 28).

We used the crystal structure of the Fn3 tandem A77-A78 domains (23) (3LPW.pdb) from the part of titin in the C-zone region to create models of titin and cMyBP-C. Each Fn3 domain is also homologous to Ig domains and is thus likely to be similar in structure particularly at the resolution of our current analysis (~28 Å). The titin model consists of a series of 11 appropriately spaced domains: two parallel copies were docked into the region alongside the 2,3,1 crown sequence of myosin heads extending 429 Å along the filament. We considered it likely that two strands could be side by side and in contact and indeed these match the density well (yellow in Fig. 4). We also used the Fn3 structure to fit three further domains which are sandwiched between the titin and the myosin head pair on crown 1 (pink in Fig. 4). It is likely that these are the C-terminal part of cMyBP-C, domains C8, C9 and C10. With this fit, these domains run parallel to the myosin filament axis in agreement with Squire et al (29) and not as a collar as suggested by Moolman-Smook *et al* (30). With this arrangement, there is an apparent interaction between the C10 domain of cMyBP-C and the motor domain of the free head of crown 1.

DISCUSSION

The structure described here for the human cardiac myosin filament in the normal (un-diseased) state is an essential starting point from which to understand the mechanisms of various cardiac diseases, in particular the effects of mutations in myosin, C-protein and titin associated with different cardiomyopathies. The current analysis shows a substantial improvement in the resolution and level of detail compared to previous studies of vertebrate striated muscle myosin filaments and allows detailed modelling of myosin heads and accessory proteins to define their interactions. Using a negative-stain approach we have achieved a degree of resolution and detail which approaches that obtained with frozen-hydrated preparations of highly ordered invertebrate myosin filaments which allow helical averaging (9, 10). We have been able to exploit the high level of detail to demonstrate that the myosin head pairs in each crown adopt the off state

conformation previously identified in smooth muscle myosin (11) and tarantula myosin filaments (9, 10). These observations are consistent with previous analysis of mouse cardiac myosin filaments at lower resolution (16) which identified the off-state conformation on crowns 1 and 3. These studies, however, were unsuccessful in recovering head pair density on crown 2 and it was suggested that this was due to higher mobility. The higher resolution in the current analysis allows us to recognise the off state head pair conformation on crown 2 and identify the orientation of the head pair by docking. It is apparent that recovery of density for the head pair is less complete on level 2, consistent with the earlier suggestion of increased mobility in this region. Increased mobility on crown 2 may be a consequence of the pattern of intermolecular interactions between crowns, since crown 2 lacks the interaction of its free head motor domain with the lever arm of the adjacent crown. The docked locations for titin and cMyBP-C described here are broadly consistent with previous proposals (16). However, the enhanced resolution of the current study makes explicit docking possible and allows the development of a molecular model.

The locations we identify for the myosin heads are quite close to the backbone and groupings of 3 crowns show well defined interactions between myosin head pairs in adjacent crowns. A head conformation recently identified biochemically has been called the super-relaxed state (SRX) in which the myosin ATPase activity is inhibited (31-33). It was concluded that the myosin heads in the SRX state are strongly stabilised on the backbone of the thick filament and have the J-like motif (11). It could well be this structure, with many of the heads making strong (sometimes blocking) interactions with their neighbours, that we have captured in our cardiac myosin filament preparation.

MATERIALS AND METHODS

Chemicals. Type III lyophilized powder elastase from porcine pancreas (code E0127), TPCK (code T4376), aprotinin from bovine lung (code A1153), pepstatin A from microbial source (code P5318), trypsin inhibitor from *Glycine max* (soyabean) (code T6522), PMSF (code P7626) were obtained from Sigma-Aldrich Chemicals, U.K. Leupeptin (code 4041) was obtained from PeptaNova GmbH. The elastase obtained from Sigma-Aldrich with code E0127 had an elastase content of 55-85%, elastase enzymatic activity ≥ 4% units/mg and trypsin activity ≤ 200 units/mg.

Isolation of myosin filaments from human heart muscle. Myosin filaments were isolated from human ventricular muscle under relaxing conditions (34). To avoid chloride induced disorder of myosin heads (35), $MgCl_2$ was replaced by MgAc in both the relaxing solution and rinsing solution for EM grids. Similarly, KCl was replaced by NH_4Ac in the EM rinsing solution. Ventricular muscles removed from donor human hearts were frozen and stored in liquid nitrogen until use. Small muscle pieces, about 80 mg, were dissected and thawed for 30 minutes in relaxing solution containing 100 mM NaCl, 2mM EGTA, 5 mM MgAc, 1mM dithiothreitol, 7mM phosphate buffer, 10 mM creatine phosphate, 5.0 mM ATP and a proteolytic inhibitors cocktail (36) (pH 6.8). The proteolytic inhibitors cocktail had four components: N-p-Tosyl-L-Phenylalanine Chloromethyl Ketone (TPCK), leupeptin, aprotinin and pepstatin A, each at a concentration of 0.004 mg/ml in the final volume of the relaxing solution. Samples were cut with a razor blade into small pieces and then teased with a pair of forceps into fine bundles 0.5 mm or less in diameter on a microscope slide and stirred for 1 hour in 10 ml of fresh relaxing solution to ensure full relaxation (assessed in the light microscope as showing long uncontracted sarcomeres). Myosin filaments were released by incubation for 3 minutes in 0.22 mg/ml elastase and 0.44 mg/ml trypsin inhibitor in a relaxing solution containing [100 mM NaCl, 2mM EGTA, 5 mM MgAc, 1mM dithiothreitol, 7mM phosphate buffer, 10 mM creatine phosphate, 5.0 mM ATP and a proteolytic inhibitor cocktail comprising five components: TPCK, leupeptin, aprotinin, pepstatin A and trypsin inhibitor, each at a concentration of 0.004 mg/ml in the final volume of the relaxing solution] (pH 6.8). The reaction was stopped by transfer into the same buffer but with 1mM PMSF and no elastase. After vigorous shaking by hand for 3 minutes and then gentle pipetting, the muscle broke up yielding a suspension of separated thick and thin filaments. The suspension was centrifuged for 2 minutes at 3000 rpm using an Eppendorf Centrifuge 5415C and EM grids were made using the supernatant.

Negative staining and Electron Microscopy. 5 µl of the isolated myosin filament suspension was applied to carbon-coated (5-7 nm thickness) 400-mesh copper grids coated with perforated Formvar and left for 10 sec. The grids were rinsed sequentially with eight drops of 50 mM NH_4Ac, 1 mM EGTA, 1 mM MgAc, 1mM dithiothreitol, 1 mM ATP and 2mM imadazole buffer at pH 6.8 and then five drops of 1% uranyl acetate and 0.025% glycerol (37, 38). Samples

were blotted with filter paper after each drop of uranyl acetate stain except for the last drop of stain, which was left on the grid for 30 sec. Most of the stain was then removed with filter paper and the grid rapidly dried with a hair dryer. Samples were imaged at room temperature in an FEI Tecnai TF20 electron microscope at an accelerating voltage of 200 kV, in low dose mode with an exposure of ~100 e^{-} $Å^{-2}$, a nominal magnification of ×29,000 and an underfocus chosen to place the first minimum in the contrast transfer function at ~17 Å. Images were recorded using a Tietz F415 (4 k × 4 k) CCD camera and fields were binned by a factor of two resulting in a calibrated sampling of 17 μm per pixel (equivalent to 5.86 Å sampling in the specimen). Only filaments lying over holes were used in the current analysis.

Preparation of filament segments and three-dimensional analysis. CCD frames were collected and evaluated using MRC (39), IMAGIC (40) and locally developed software. Regions were selected which contained intact half-filaments which were relatively straight, minimally overlapped by actin and other myosin filaments, and with readily identifiable bare-zones (Fig. S1A,B). Whole myosin filaments were cut into two half filaments (each including the whole bare-zone) and half filaments were oriented with their bare-zones pointing vertically downwards (Fig. S1B). From the C-zone of these half-filaments, segments were extracted, each segment being centred on a 429 Å repeat and being 950 Å in length (just over 2 x 429 Å repeats). Three-dimensional analysis was conducted using the approach previously described for vertebrate myosin filaments (13, 14). During the later stages of the refinement we used a brute force multireference alignment program which performs rotational and translational alignment independently. We also used a locally developed Fourier space three-dimensional reconstruction program (41). Docking of the atomic coordinates into the density was done manually with PyMOL (The PyMOL Molecular Graphics System, Version 1.2r3pre, Schrödinger, LLC) and then docking was refined computationally using the VEDA (http:/mem.ibs.fr/GAEL/index.html) interface to URO (19).

ACKNOWLEDGEMENTS

This work was supported by a British Heart Foundation Fellowship to HA (#FS/07/017/22951). RWK was supported by a Minorities Basic Research Support Grant 5SC1HL96017 from the National Institutes of Health, and, in part, by funding from a “Research Centers in Minority Institutions” Award G12RR-03051, from the National Center for Research Resources, National Institutes of Health

REFERENCES

1.Huxley HE (1963) Electron Microscope Studies on the Structure of Natural and Synthetic Protein Filaments from Striated Muscle. *J Mol Biol* 7:281-308.

2.Squire JM (1972) General model of myosin filament structure. II. Myosin filaments and cross-bridge interactions in vertebrate striated and insect flight muscles. *J Mol Biol* 72(1):125-138.

3.Labeit S, Kolmerer B (1995) Titins: giant proteins in charge of muscle ultrastructure and elasticity. *Science* 270(5234):293-296.

4.Trinick J (1996) Titin as a scaffold and spring. Cytoskeleton. *Curr Biol* 6(3):258-260.

5.Offer G, Moos C, Starr R (1973) A new protein of the thick filaments of vertebrate skeletal myofibrils. Extractions, purification and characterization. *J Mol Biol* 74(4):653-676.

6.Bennett P, Craig R, Starr R, Offer G (1986) The ultrastructural location of C-protein, X-protein and H-protein in rabbit muscle. *J Muscle Res Cell Motil* 7(6):550-567.

7.Craig R (2012) Isolation, electron microscopy and 3D reconstruction of invertebrate muscle myofilaments. *Methods* 56(1):33-43.

8.Squire JM (2009) Muscle Myosin Filaments: Cores, Crowns and Couplings. *Biophysical Reviews* 1:149-160.

9.Woodhead JL, *et al.* (2005) Atomic model of a myosin filament in the relaxed state. *Nature* 436(7054):1195-1199.

10.Alamo L, *et al.* (2008) Three-dimensional reconstruction of tarantula myosin filaments suggests how phosphorylation may regulate myosin activity. *J Mol Biol* 384(4):780-797.

11.Wendt T, Taylor D, Trybus KM, Taylor K (2001) Three-dimensional image reconstruction of dephosphorylated smooth muscle heavy meromyosin reveals asymmetry in the interaction between myosin heads and placement of subfragment 2. *Proc Natl Acad Sci U S A* 98(8):4361-4366.

12.AL-Khayat HA, Morris EP, Squire JM (2004) Single Particle Analysis: A new approach to solving the 3D structure of myosin filaments. *J Muscle Res Cell Motil* 25(8):635-644.

13.AL-Khayat HA, Morris EP, Kensler RW, Squire JM (2006) 3D structure of relaxed fish muscle myosin filaments by single particle analysis. *J Struct Biol* 155(2):202-217.

14.AL-Khayat HA, Morris EP, Kensler RW, Squire JM (2008) Myosin filament 3D structure in mammalian cardiac muscle. *J Struct Biol* 163(2):117-126.

15.AL-Khayat HA, Morris EP, Squire JM (2009) The 7-stranded structure of relaxed scallop muscle myosin filaments: support for a common head configuration in myosin-regulated muscles. *J Struct Biol* 166(2):183-194.

16.Zoghbi ME, Woodhead JL, Moss RL, Craig R (2008) Three-dimensional structure of vertebrate cardiac muscle myosin filaments. *Proc Natl Acad Sci U S A* 105(7):2386-2390.

17.Seidman CE, Seidman JG (2011) Identifying sarcomere gene mutations in hypertrophic cardiomyopathy: a personal history. *Circ Res* 108(6):743-750.

18.Marston S, (2011) How do mutations in contractile proteins cause the primary familial cardiomyopathies. *J Cardiovasc Trans Res* 4:245-255.

19.Navaza J, Lepault J, Rey FA, Alvarez-Rua C, Borge J (2002) On the fitting of model electron densities into EM reconstructions: a reciprocal-space formulation. *Acta Crystallogr D Biol Crystallogr* 58(Pt 10 Pt 2):1820-1825.

20.Dominguez R, Freyzon Y, Trybus KM, Cohen C (1998) Crystal structure of a vertebrate smooth muscle myosin motor domain and its complex with the essential light chain: visualization of the pre-power stroke state. *Cell* 94(5):559-571.

21.Liversage AD, Holmes D, Knight PJ, Tskhovrebova L, Trinick J (2001) Titin and the sarcomere symmetry paradox. *J Mol Biol* 305(3):401-409.

22.Knupp C, Luther PK, Squire JM (2002) Titin organisation and the 3D architecture of the vertebrate-striated muscle I-band. *J Mol Biol* 322(4):731-739.

23.Bucher RM, Svergun DI, Muhle-Goll C, Mayans O (2010) The structure of the FnIII Tandem A77-A78 points to a periodically conserved architecture in the myosin-binding region of titin. *J Mol Biol* 401(5):843-853.

24.LeWinter MM, Granzier H (2010) Cardiac titin: a multifunctional giant. *Circulation* 121(19):2137-2145.

25.Kruger M, Linke WA (2011) The giant protein titin: a regulatory node that integrates myocyte signaling pathways. *J Biol Chem* 286(12):9905-9912.

26.Tskhovrebova L, Trinick J (2010) Roles of Titin in the Structure and Elasticity of the Sarcomere. *Journal of Biomedicine and Biotechnology*.

27.Yasuda M, Koshida S, Sato N, Obinata T (1995) Complete primary structure of chicken cardiac C-protein (MyBP-C) and its expression in developing striated muscles. *J Mol Cell Cardiol* 27(10):2275-2286.

28.Gautel M, Zuffardi O, Freiburg A, Labeit S (1995) Phosphorylation switches specific for the cardiac isoform of myosin binding protein-C: a modulator of cardiac contraction? *Embo J* 14(9):1952-1960.

29.Squire JM, Luther PK, Knupp C (2003) Structural evidence for the interaction of C-protein (MyBP-C) with actin and sequence identification of a possible actin-binding domain. *Journal of Molecular Biology* 331(3):713-724.

30.Moolman-Smook J, *et al.* (2002) Identification of novel interactions between domains of myosin binding protein-C that are modulated by hypertrophic cardiomyopathy missense mutations. *Circulation Research* 91(8):704-711.

31.Stewart MA, Franks-Skiba K, Chen S, Cooke R (2010) Myosin ATP turnover rate is a mechanism involved in thermogenesis in resting skeletal muscle fibers. *Proceedings of the National Academy of Sciences of the United States of America* 107(1):430-435.

32.Hooijman P, Stewart MA, Cooke R (2011) A New State of Cardiac Myosin with Very Slow ATP Turnover: A Potential Cardioprotective Mechanism in the Heart. *Biophysical Journal* 100(8):1969-1976.

33.Naber N, Cooke R, Pate E (2011) Slow Myosin ATP Turnover in the Super-Relaxed State in Tarantula Muscle. *Journal of Molecular Biology* 411(5):943-950.

34.Kensler RW, Harris SP (2008) The structure of isolated cardiac Myosin thick filaments from cardiac Myosin binding protein-C knockout mice. *Biophys J* 94(5):1707-1718.

35.Kensler RW, Levine RJ (1982) An electron microscopic and optical diffraction analysis of the structure of Limulus telson muscle thick filaments. *J Cell Biol* 92(2):443-451.

36.Sellers JR (1981) Phosphorylation-dependent regulation of Limulus myosin. *J Biol Chem* 256(17):9274-9278.

37.Stewart M, Kensler RW (1986) Arrangement of Myosin Heads in Relaxed Thick Filaments from Frog Skeletal-Muscle. *Journal of Molecular Biology* 192(4):831-851.

38.Kensler RW, Stewart M (1983) Frog Skeletal-Muscle Thick Filaments Are 3-Stranded. *Journal of Cell Biology* 96(6):1797-1802.

39.Crowther RA, Henderson R, Smith JM (1996) MRC image processing programs. *Journal of Structural Biology* 116(1):9-16.

40.van Heel M, *et al.* (2000) Single-particle electron cryo-microscopy: towards atomic resolution. *Quarterly Reviews of Biophysics* 33(4):307-369.

41.da Fonseca PCA, He J, Morris EP (2012) Molecular Model of the Human 26S Proteasome. *Molecular Cell* 46(1):54-66.

42.Van Heel, M, Schatz, M (2005) Fourier shell correlation threshold criteria. *Struct Biol* 151:250-262.

	Axial r ise expected	Axial rise found	Azimuthal rotation expected	Azimuthal rotation observed	Change in tilt angle with respect to level 1
	Relative positions o f head pa ir centres				
Crown 1 t o Crown 2	**143**	**132**	**40**	**60**	**-19**
Crown 2 t o Crown 3	**143**	**148**	**40**	**35**	**0**
Crown 3 t o Crown 1	**143**	**149**	**40**	**25**	**19**
	Relative positions o f head origins				
Crown 1 t o Crown 2	**143**	**133**	**40**	**58**	**NA**
Crown 2 t o Crown 3	**143**	**148**	**40**	**30**	**NA**
Crown 3 t o Crown 1	**143**	**148**	**40**	**32**	**NA**

Table 1: Comparison of Crown axial spacings/ separations, and angular/ azimuthal rotations as well as the change in tilt angle in going from one Crown level to the next. The top figures refer to the centre of mass of the head pairs and the bottom figures to their origins where they meet S2. Positive angles in the tilt values are in the clockwise direction. (NA: not applicable).

FIGURE LEGENDS

Figure 1: (A-D) Surface views of 3D reconstructions of the human cardiac myosin filament obtained by the single-particle EM analysis and displayed using PyMOL showing a length of a full 429 Å repeat. The reconstruction is shown in two interleaved stereo views (A,C) and (B,D). The stereo views are rotated by 25˚ relative to each other around the filament axis, such that in (A,C), a myosin head pair on level 1 is facing the viewer and in (B,D), a myosin head pairs on level 3 is facing the viewer. Note that the two views in (A,C) and (B,D) are quite distinct because of the different perturbations in the crowns. The triangular-shaped configurations for the three head pairs on each crown level are shown in yellow, blue and pink for levels 2, 3 and 1, respectively, in (C,D). The bare-zone is at the bottom of the map in all the four views. (E) Crystal structure for the head pair (11). The blocked and free heads are colour-coded as in (9-11). Blocked head: motor domain, green; essential light chain, orange; regulatory light chain, yellow. Free head: motor domain, cyan; essential light chain, pink; regulatory light chain, beige.

Figure 2: (A,C) Two stereo views of the map shown in Fig. 1 rotated by 25˚ with respect to each other around the filament axis. Fitting of the atomic model of myosin heads in the off-state (after splitting the two heads from Alamo et al (10)) to the head motif in crowns 2, 3 and 1. The majority of the atomic structures for the head pairs are well-contained within the density map on crowns 3 and 1, but less on crown 2, especially for the two lever arms parts. The S2 is also fitted as described in the text. (B,D) same views as in (A,C) but shown without the 3D map. S2 is shown in red and the bare-zone direction is towards the bottom in all views.

Figure 3: (A) Two interleaved stereo views rotated by 30˚ with respect to each other showing the head pairs on successive crowns along one of the three strands of the human cardiac myosin filament.

Head pairs in the 2,3,1 crown sequence are quite closely connected while there is a distinct gap between crowns 1 and 2. (B) No intermolecular interaction is seen between the head pairs in crowns 1 and 2. (C) The head pairs on level 3 and 2 are connected through an interaction between the ELC of the blocked head on crown 2 and the motor domain of the free head on crown 3. (D) A different type of intermolecular connection is observed between crowns 3 and 1 which is mediated by the interaction between the RLC of the blocked head on crown 3 and the motor domain of the free head on crown 1. S2 is shown in red and the bare-zone direction is towards the bottom in all views.

Figure 4: The final 3D map (Fig.1) shown with myosin head pairs, S2 (red), titin (yellow) and the three c-terminal domains of cMyBP-C (C8-C10) (magenta). Bare-zone direction is towards the bottom.

SUPPLEMENTARY INFORMATION

Fig. S1 (A) Overview electron micrograph of isolated myosin filaments (M) from the ventricular muscle of normal (un-diseased) human heart in the relaxed state, viewed in negative stain over a hole in the support film. Some actin filaments (A) can be seen in the background. The helical arrays of myosin heads are evident in each half of the bipolar myosin filaments (scale bar 2000 Å). (B) Left: Schematic diagram showing the different A-band regions within the myosin half-filament as defined by Sjostrom and Squire (1977a,b) starting with the half M-band at the bottom, then the half bare-zone (M-region), the P-zone and the C-zone. Particles were selected from the C-zone only, each particle being just over 2 x 429 Å repeats long and with a C-protein stripe (black circle) in the middle. Right: Typical half-filament selected from the micrograph such as in (A), shown with the M-region (bare-zone) towards the bottom and showing the characteristic 429 Å axial repeat. The first particle was selected at the position shown by a red square of size 160 pixels, equivalent to just over 2 x 429 Å, and whose edge was at a distance 2040 Å from the middle of the M-band. The second particle was selected after stepping by a distance of 429 Å from the first and so on. (C) Calculated Fourier transforms of the half-filament shown in (B: right). Orders of the 429 Å repeat are shown in white numbers. The spacing of the 6^{th} order of the 429 Å repeat, the 71.5 Å meridional reflection, was used to calibrate the magnification and to adjust the sampling of each half-filament from all the different micrographs to be exactly 5.94 Å/pixel. This 6^{th} order meridional reflection was particularly strong in most of the Fourier transforms. The 11^{th} and 12^{th} orders of the 429 Å repeat corresponding to 39 Å (the titin sub-repeat) and 35.75 Å resolution, respectively, is also visible. (C) Zoomed view of the area boxed in (C) to show orders up to 16^{th} corresponding to a resolution of 26.81 Å.

Fig. S2 Distribution of the viewing angles assigned to the 285 particles; the spread in γ (angle about the filament axis) is -58° to 59° (which theoretically lies between -60° and +60° because of the C3 point group symmetry) and in β (out of the plane of the grid) is between 80° to 100°. This plot,

therefore, shows that there is a satisfactory spread of viewing angles with which to generate a 3D reconstruction and hence confirms the reliability/validity of the reconstruction.

Fig. S3 Estimation of the resolution of the reconstruction using a Fourier Shell Correlation (FSC) plot (solid line) obtained by comparing two independent reconstructions each representing half the dataset of the final 3D map shown in Figure 1. Resolution is assessed with respect to the half-bit criteria (dashed line) according to the definitions of van Heel and Schatz (42) and the 0.5 FSC (horizontal dot-dashed line), confirming that the resolution is valid up to 28.0 Å.

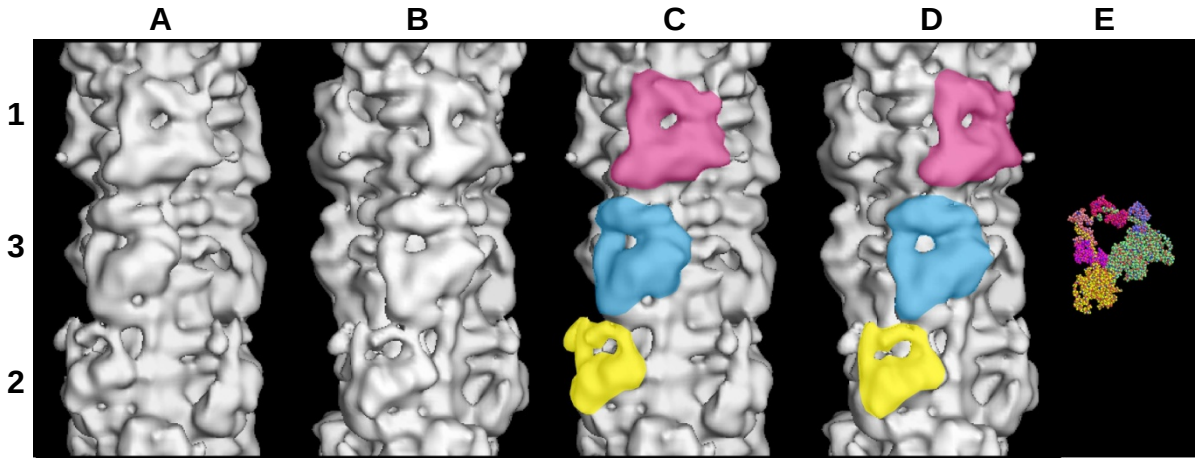

Figure 1

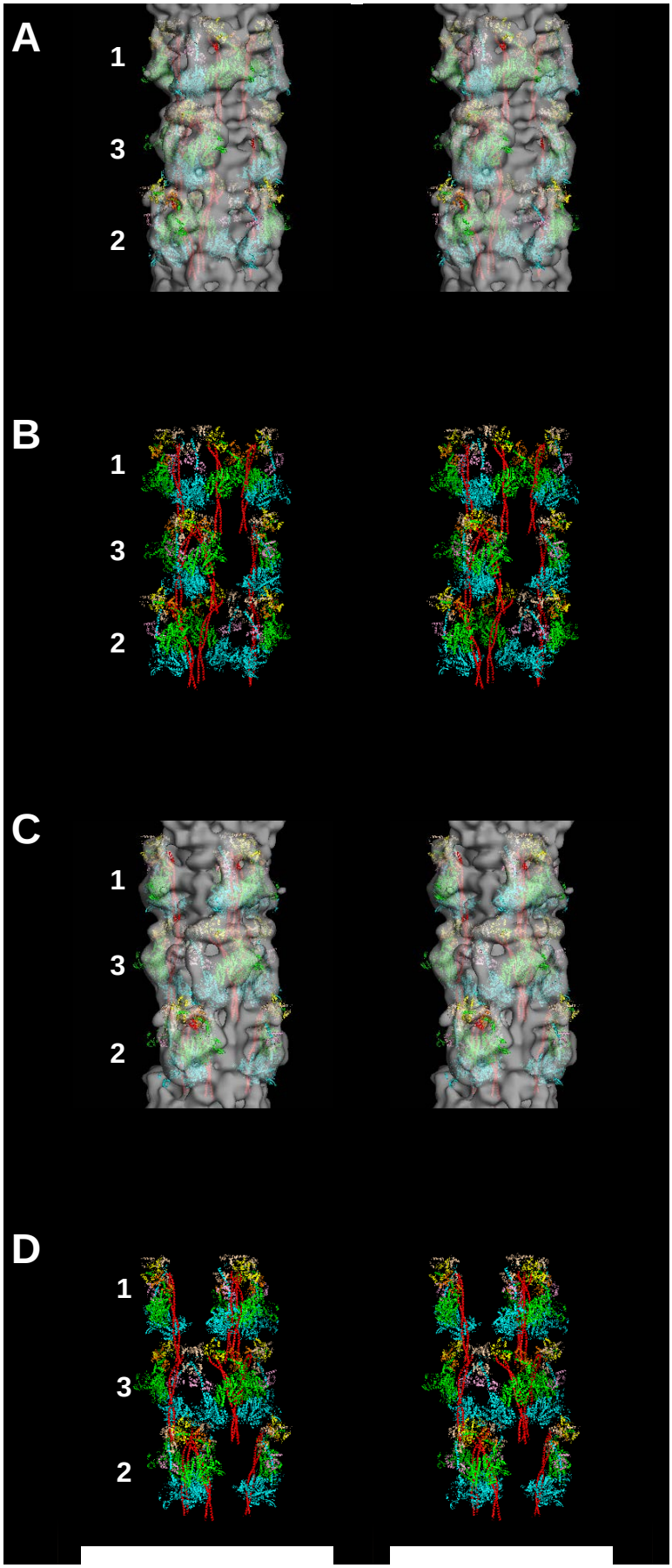

Figure 2

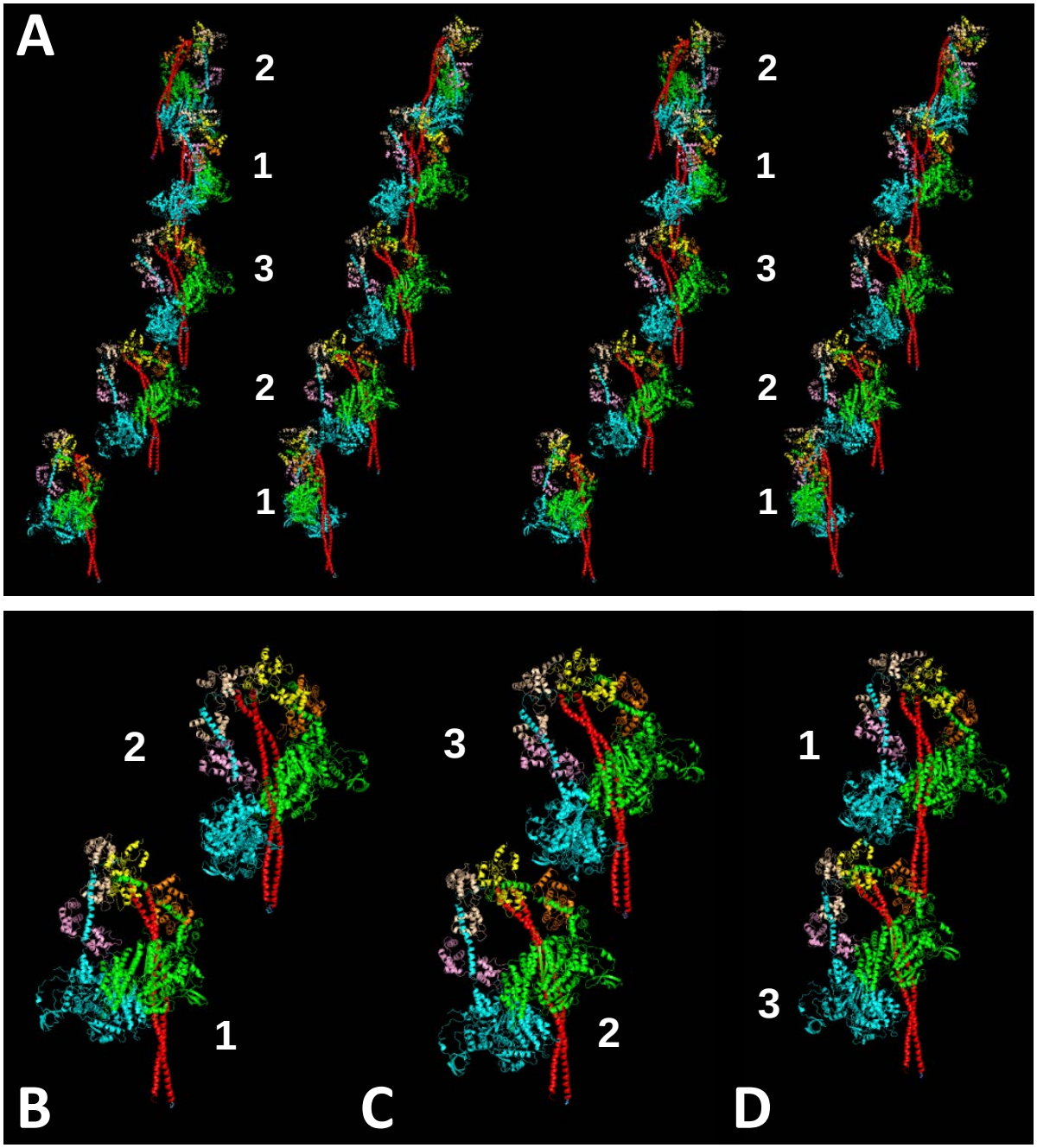

Figure 3

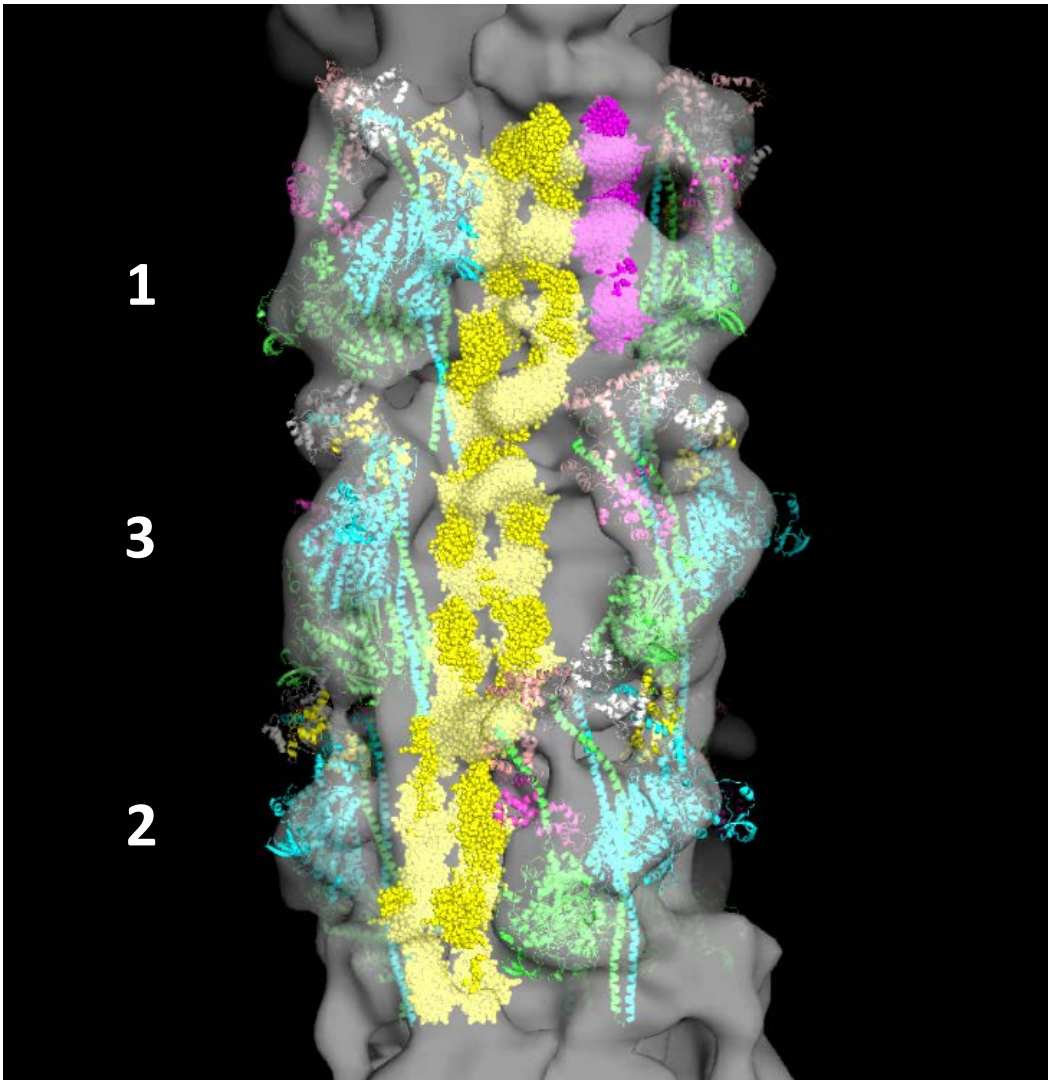

Figure 4

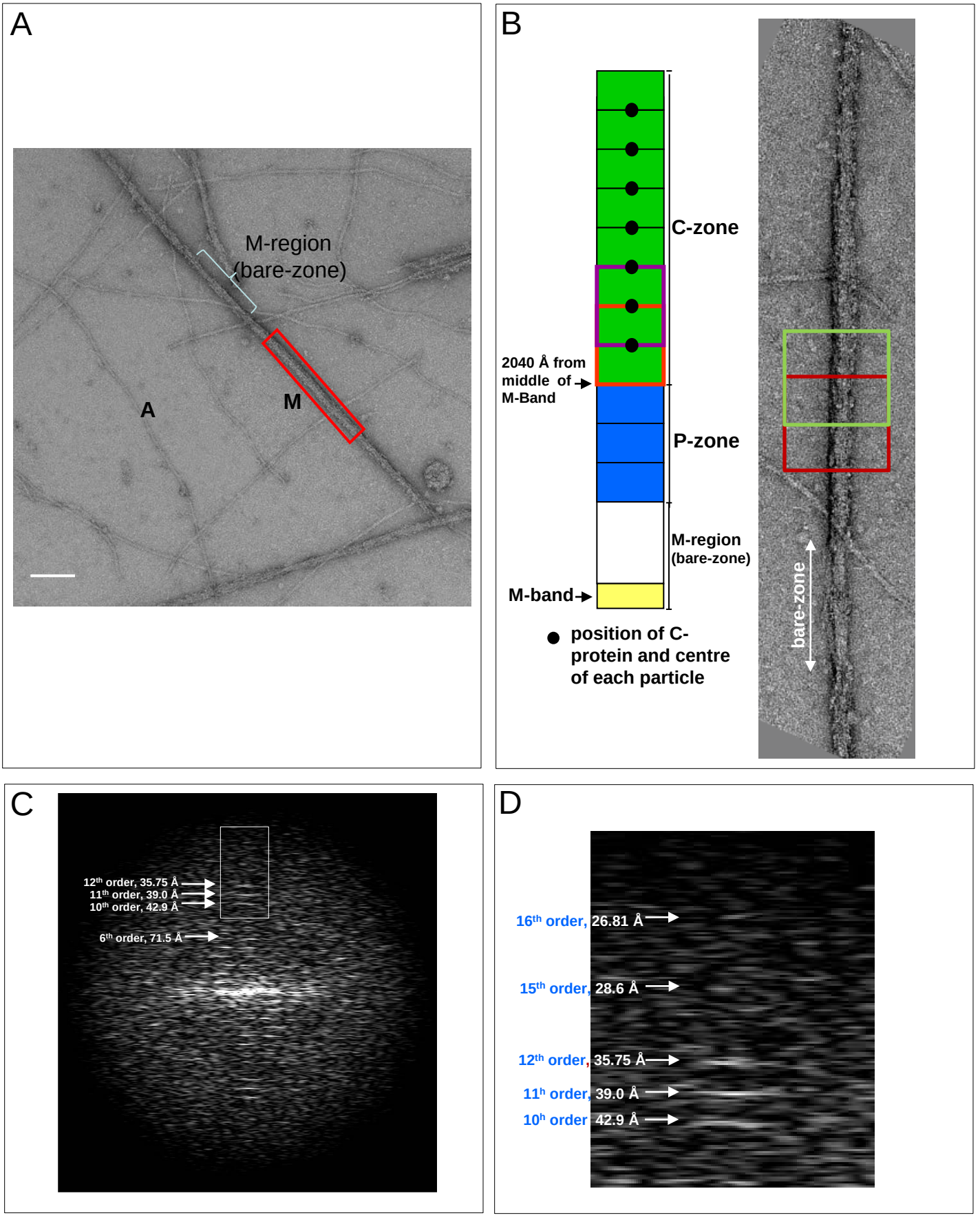

Supplementary Figure 1

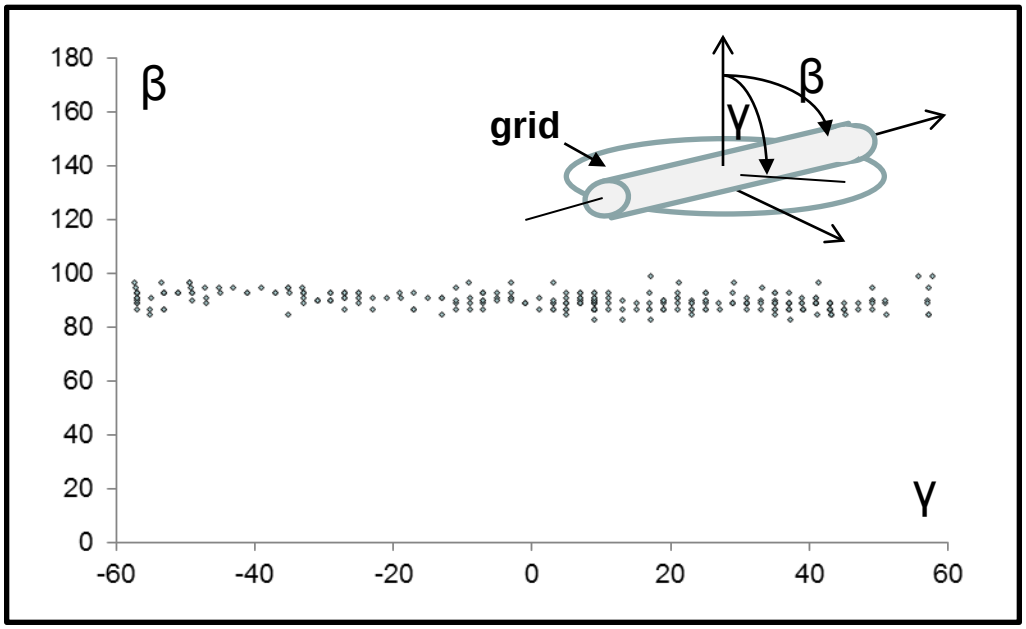

Supplementary Figure 2

Supplementary Figure 3